Supplemental Document

Biomedical Optics EXPRESS

Deriving high contrast fluorescence microscopy images through low contrast noisy image stacks: supplement

Sebastian Acuña,[1,3,*] Mayank Roy,[2,3] Luis E. Villegas-Hernández,[1] Vishesh K. Dubey,[1] Balpreet Singh Ahluwalia,[1] and Krishna Agarwal[1]

[1] *Department of Physics and Technology, UiT The Arctic University of Norway, 9010 Tromsø, Norway*
[2] *Indian Institute of Technology (Indian School of Mines), Dhanbad 826004, India*
[3] *Shared co-authors*
[*] *sebastian.acuna@uit.no*

Supplement DOI: https://doi.org/10.6084/m9.figshare.14544363

Parent Article DOI: https://doi.org/10.1364/BOE.422747

Supplementary notes: Deriving high contrast fluorescence microscopy images through low contrast noisy image stacks

*sebastian.acuna@uit.no

Note S1. Tissue sample preparations

Full term human placenta was collected immediately after delivery. A written consent from the participants was obtained according the protocol approved by the Regional Committee for Medical and Health Research Ethics of North Norway (REK Nord reference no. 2010/2058-4). All the samples were anonymized. Chorionic tissue blocks of 1 mm^3 were dissected, washed and preserved following the Tokuyasu method for cryo-ultramicrotomy, as described elsewhere [1]. Myocardial samples (pig-heart tissue) were extracted from anesthetized pigs through a biopsy needle. After dissection into 1 mm^3, the samples were further washed and preserved identically as the placental samples, including storage in liquid nitrogen. The collection of the pig hear samples followed the ethical protocols approved both by the Animal Welfare Board at UiT - The Arctic University of Norway (NO-9037 Tromsø, Norway), and the Norwegian Food Safety Authority Mattilsynet (NO-9008 Tromsø, Norway). The cryo-preserved placental tissues were sectioned into thin slices of 1 µm using a cryo-ultramicrotome (EMUC6, Leica Microsystems) and collected with a wire loop containing a 1:1 cryo-protectant mixture of 2.3M sucrose and 2% methylcellulose. Thereafter, the sections were placed onto poly-L-lysine coated microscope coverslip (#1.5) and labelled against F-actin, lipid membranes and nuclei using Phalloidin-Atto647N (1:100 solution in phosphate-buffered saline (PBS)), CellMask Orange (CMO) (1:2000 solution in PBS), and Sytox Green (10 µM in PBS), respectively. The pig heart samples were sectioned into 100 nm sections and placed onto a photonic chip [2] before further labeling against lipid membranes and nuclei using CMO (1:2000 solution in PBS), and Sytox Green (10 µM in PBS), respectively. All the labelling and mounting steps were identical as for the placental sections. The tissue sections were imaged using a DeltaVision OMX V4 Blaze microscope imaging system (OMX) (GE Healthcare) was used. The OMX microscope allowed both epi-fluorescence and structured illumination microscopy (used as a reference). The OMX was equipped with a 60X/NA1.42 oil-immersion objective lens (Olympus). For contrast enhancement, image stacks were obtained in epi-fluorescence (EPI) mode by matching the imaging channels of the microscope to the excitation wavelength of each fluorophore. For reference, structured illumination mode (SIM) images were also acquired. Laser illumination (488 nm, 568 nm, 642 nm) was used for SIM images, while the proprietary InsightSSI™light sources were used for the EPI acquisition. The 642 nm channel was used for imaging F-actin (labelled with Phalloidin-Atto647N), and the 568 nm channel was used for imaging lipid membranes (stained with CMO). Similarly, the 488 nm channel was used for imaging nuclear content (stained with Sytox Green). Refractive index matching was performed before image acquisition. This was performed by changing the immersion oil and observing the orthogonal views of z-stack images until the point-spread function (PSF) of single emitters showed symmetrical shapes at two sides of the focal plane. Typical refractive indices used in the study ranged from 1.514 to 1.516. The image acquisition parameters were optimized according to the desired reconstruction technique. For the reference SIM images, the maximum intensity count was set to approximately 10000 for CMO, requiring acquisition times within 10 ms and 35 ms per frame. On the other hand, the intensity count in EPI mode was set below 3000, which allowed for shorter acquisition times (between 4 ms and 10 ms per frame). For the reference SIM images, the specimens were imaged at several focal planes at consecutive sapling z-steps of 125 nm. A total of 15 frames per imaging channel were acquired for each z-plane, corresponding to 5 phases and 3 orientations necessary for SIM

reconstruction. As for EPI mode, the focal plane was fixed while several images were recorded.

Note S2. Contrast quantification

To measure contrast improvement quantitatively, we tried several strategies. While in literature comparisons are obtained by measuring PSNR or SSIM, both methods require ground-truth which is unavailable for experimental fluorescently labeled samples. Therefore, we have tried blind methods as metrics that only rely on a single image. We have collected some of the metrics in the following tables for the four samples presented in our work.

BRISQUE [3] is a blind image quality assessment algorithm available in MATLAB that analyzes the distribution of intensities across the images with the images of the same distribution and distortions (images that the algorithm has been trained with). These images have been manually evaluated in terms of quality, with 0 being the best and 100 the poorest. Therefore, an improved image should display a smaller BRISQUE index. However, we note that the algorithm was applied with the default MATLAB's model for BRISQUE which may not be suitable for microscopy images. The second metric corresponds to the standard deviation of all the intensities as a measure of dispersedness. We would expect a good image to have a larger value as it would mean that more range is used. On the contrary, an image with concentrated intensities would display a low value. The third metric is entropy which also measure the distribution and is a measure of the information contained in the image.

In the case of the In-vitro actin filaments (Table S1), we empirically observed that the best results were obtained by CE1 and C1S. However, from the BRISQUE analysis only the MUSICAL results showed improvement, while something similar occurs for standard deviation and entropy whose values are actually lower. On the other hand, ACsN achieves a better ACsN index, probably because of how the resulting image is smoother and therefore closer to natural objects. Similar results are observed for RL deconvolution. In terms of entropy, only MUSICAL achieves a large entropy which can be due to the high intensity of the reconstructed signal and very low background. This is expected as the indicator function of MUSICAL can produce very values in cases where the denominator becomes small.

Table S1. Quantification of results for In-vitro F-actin sample. BRISQUE: range of values is [0,100], lower is better. Standard deviation: higher values are better. Entropy: higher values is better.

Method	Threshold	BRISQUE	Standard deviation	Entropy
CE1	-0.67	57.033263	0.298227	0.464771
CE2	-0.67	45.233701	0.082632	0.059277
CE1s	——	45.933282	0.155533	0.167627
CE2s	——	52.747246	0.26646	0.391211
MUSICAL	-0.67	50.616861	0.035348	1.384741
ACsN	——	46.198068	0.228289	0.307909
Mean	——	53.020122	0.325196	0.529922
RL	——	44.579228	0.068589	0.043316

On the sample of microtubules (Table S2), CE1 and CE2, MUSICAL and RL gets better values. However, they differ in entropy as CE1 shows the largest among the four. In terms of standard deviation, CE1 is again among the best ranked and therefore, an indicator that its

intensity distribution could be in fact improved. This matches our empirical observations.

Table S2. Quantification of results for microtubules in U2OS cells. BRISQUE: range of values is [0,100], lower is better. Standard deviation: higher values are better. Entropy: higher values is better.

Method	Threshold	BRISQUE	Standard deviation	Entropy
CE1	-1.5	44.117168	0.44294	0.838632
CE2	-1.5	45.474566	0.2414	0.335858
CE1s	——	53.802671	0.215861	0.282117
CE2s	——	52.483188	0.471	0.917142
MUSICAL	-1.5	44.381886	0.003906	0.000266
ACsN	——	50.843798	0.307687	0.487365
Mean	——	51.734493	0.332461	0.547875
RL	——	44.429404	0.039227	0.016619

In the case of placenta (Table S3) there is almost no variation in the BRISQUE coefficient. This can be explained in most of the cases where the reconstruction shows the clear presence of villi. However, it is harder to explain for samples where the structure is not even present. In terms of stardard deviation, neither of the methods show a better value than the mean. The same occurs with the entropy.

Table S3. Quantification of results for placenta tissue sample. BRISQUE: range of values is [0,100], lower is better. Standard deviation: higher values are better. Entropy: higher values is better.

Method	Threshold	BRISQUE	Standard deviation	Entropy
CE1	-0.75	44.618227	0.101571	0.083598
CE2	-0.75	44.504435	0.056479	0.03113
CE1s	——	44.854262	0.134484	0.132504
CE2s	——	44.574906	0.10776	0.092183
MUSICAL	-0.2	44.363584	0.01	0.001473
MUSICAL	-0.75	44.400236	0.036033	0.014338
ACsN	——	44.734983	0.165759	0.185666
Mean	——	45.816136	0.232132	0.316026
RL	——	44.722878	0.142464	0.145492

The pig-heart tissue sample is maybe the worst case as the SIM image which was expected to give the best result, gives the worst, which renders BRISQUE unusable as a comparison metric for this case. However, such image also shows the best (largest) deviation and entropy which can be correlated to the better quality of the image.

From the metrics used, neither seems to be useful for comparing the contrast of the results as

Table S4. Quantification of results for pig-heart tissue sample. BRISQUE: range of values is [0,100], lower is better. Standard deviation: higher values are better. Entropy: higher values is better.

Method	Threshold	BRISQUE	Standard deviation	Entropy
SIM	——	56.0157	0.492524	0.978478
CE1	-0.38	44.689645	0.101571	0.083598
CE2	-0.38	44.44668	0.024488	0.007287
CE1s	——	44.85316	0.101208	0.083105
CE2s	——	44.386956	0.01	0.001473
MUSICAL	-0.38	45.378781	0.079279	0.055298
ACsN	——	46.231884	0.476509	0.932744
Mean	——	46.037961	0.414606	0.761125
RL	——	44.363584	0.01	0.001473

they in general did not correlated with what was observed empirically. BRISQUE could still be useful in the future provided that good fluorescence images are available for a better model.

Note S3. Contrast enhancement on simulated example

In order to achieve and quantify our contrast enhancement methods, we created a simple structure using squares. The groundtruth is shown in Fig. S1 where single emitters are placed in the perimeter of each structure, at different densities. We defined the densities in terms of the first square (labeled in blue) using a multiplier from 1 to 9 times for each case. As a result, the square at the upper-left is harder to appreciate in comparison to the one at the bottom-right. We used emission wavelength of 660 nm, numerical aperture (NA) of 1.2 and pixel size of 108 nm. The squares itself have the same size, with a side of 500 nm. The space between them is 500 nm as well. This is a distance above the resolution limit as the purpose was to analyze only contrast. Each emitters is active in average 1 every 4 frames, with a density of 100 emitters per μm. The noise is added later using a Poisson distribution in order to control the signal to background ratio. We used two values: 2 and 4. All the results are shown in Fig. S2.

The analysis was made by analyzing the profile line across the vertical line shown in blue in Fig. S2a. In these examples it is possible to observe how CE increase the contrast basically in two ways. One way is by looking to the centers of each square where it is possible to observe a deeper valley when compared to the mean. More interesting though, is the effect on the dimmer structure in the top left of the image, where CE1 allows an increase in the intensities, making its visualization easier.

In terms of the effect of the noise, CE1 is was clearly affected by it as the results get poor for a low SBR.

On the other hand, CE2 shows an interesting result as the 9 squares look similar in terms of brightness suggesting a normalization effect. However, definition is lost and a gradient effect is seen for both cases of noise, which is considered an artifact.

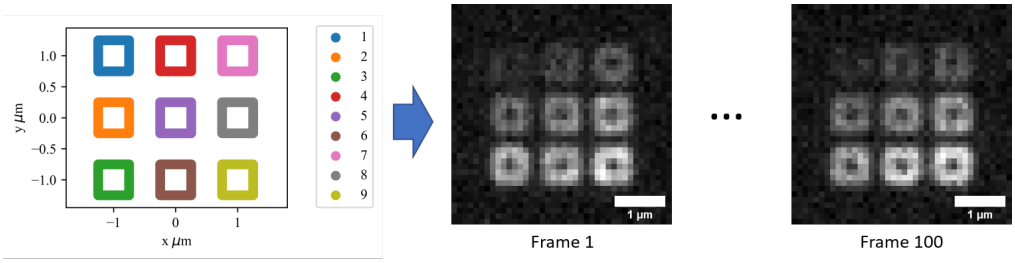

Fig. S1. Simulation of 9 flat square frames, with every square having different brightness proportional to its index (from 1 to 9).

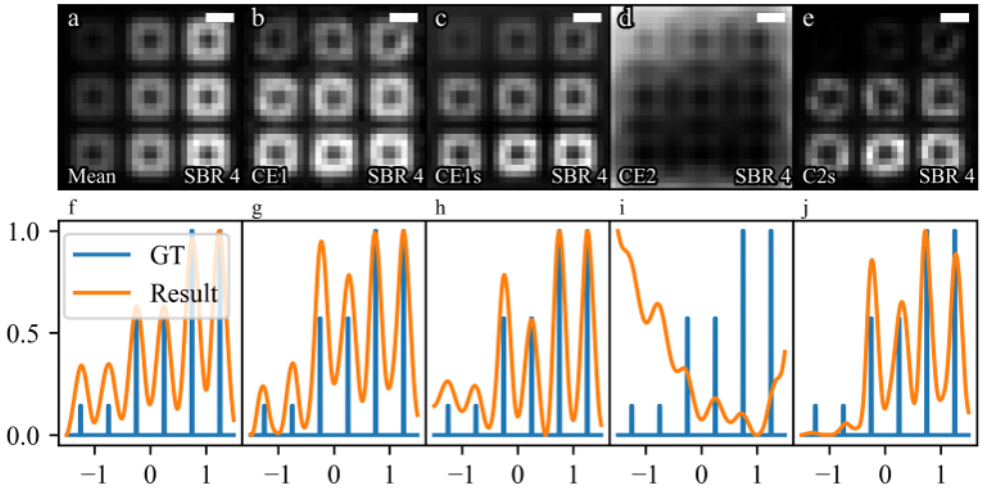

Fig. S2. Results on simulations show the effect of applying CE methods on the square sample. Scale bar is 500 nm. **a-e.** Results on sample with SBR 4. **f-j.** Profile across an horizontal line for the images shown in **a-e.**.

Note S4. Out-of-focus removal - an illustration

We show an example of 3 spherical structures as a demonstration of the out-of-focus removal of our method. The three-dimensional structure is shown in Fig. S3a. Next to it, in Fig. S3b, we display the scatter plot of emitters located at 200 nm from the focal plane at most. The surface of the spheres is filled with emitters placed randomly. The large sphere has a radius of 1 μm and a density of 1000 emitters per μm^2. The small green sphere (left) has a density of 2000 emitters μm^2 and the orange (right) has a density of 1000. Emission wavelength is fixed at 660, with NA 1.42 and pixel size of 108 nm. Each emitter is active 1 every 4 frames on average, and Poisson noised is added for each pixel independently.

In the mean image, the haze around the two small spheres is produced by out-of-focus signal coming from emitters on the large sphere. As the PSF is wider at this positions, the number of overlap signal increases at the focal plane and as a result, we obtain an overall signal that seems constant and that does not fade away after averaging. The CE methods can filter out signal with low variance resulting from a larger number of overlapping small signals and produce an increased difference between signal and background. Further, the use of g_i, i.e. the projection of the PSF in the focal plane on the ith eigenimage allows for selectively enhancing the signal which

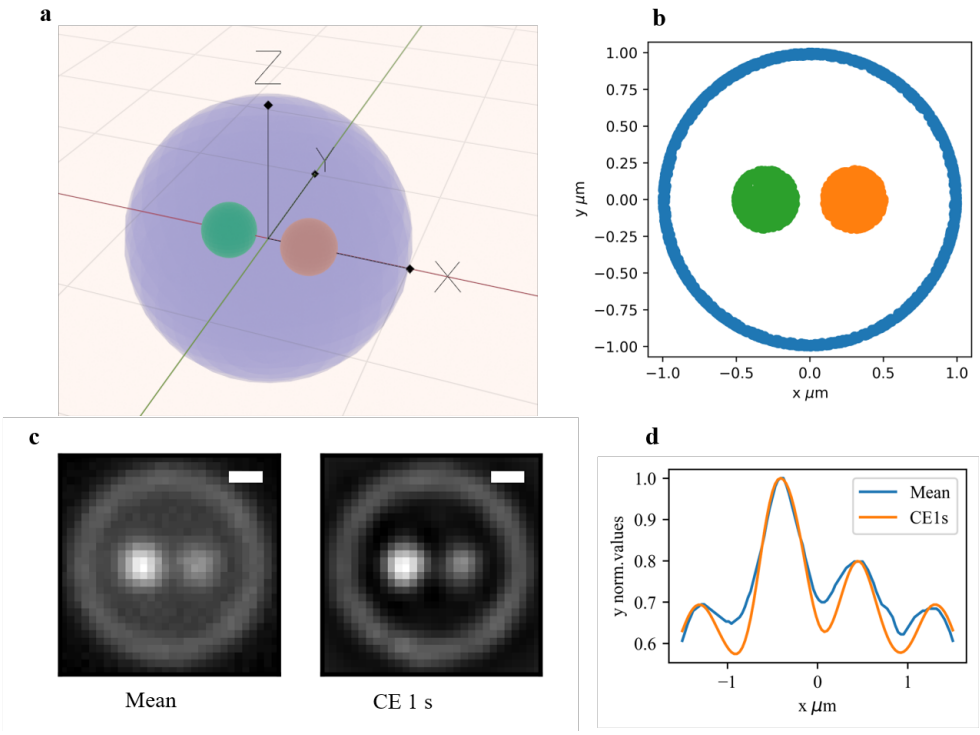

Fig. S3. Background suppression example shown on a simulation of spherical structures with labeling in the surface. The large sphere has radius 1 µm with a density of emitter of 1000 emitters per µm^2, while the small ones inside have radius 200 nm with densities 1000 and 2000 emitters per µm^2 respectively. The distance between centers of the two small spheres is 600 nm. **a.** 3D rendering of the structure of interest. The 3D scale has 1 µm in each direction. **b.** Plot of actual emitters are single points. Only the ones at a maximum distance of of 200 nm from the focal plane (the one passing for all the 3 centers are display here). **c.** Result of applying the mean and CE1s.

comes from the focal region. The effect is evident in the profile across the horizontal mid-section of the images as seen in Fig. S3d. In these curves the valleys around the signal coming from the small spheres is pronounced for CE1s, indicating the enhancement in contrast.

Note S5. Effect of incorrect estimate of the PSF - investigation of sensitivity to PSF

Considering the dataset of pig heart tissue, presented in Fig. 4 in the main article, we investigate the sensitivity of CE1s to the accurate knowledge of the PSF. We choose CE1s since it clearly presents better performance than the other indicator functions across different challenging scenarios. While the actual dataset is acquired using an objective lens of numerical aperture (NA) 1.42, we consider hypothetical situations where the NA of the objective lens is incorrectly estimated and used for constructing the CE1s image. We consider two candidates for incorrect NA, namely 1.2 and 1.6. We present the CE1s images for all the three NAs, namely 1.2, 1.42, and 1.6 in Fig. S4a-c respectively. The intensity at a cross-section of interest is plotted in Fig. S4d. It is seen that CE1s is not sensitive to the accurate knowledge or estimate of the PSF. On the other hand, the original MUSICAL [4] was comparatively more sensitive, presenting pronounced sharpening or blurring effect with the usage of higher or lower NA than the actual

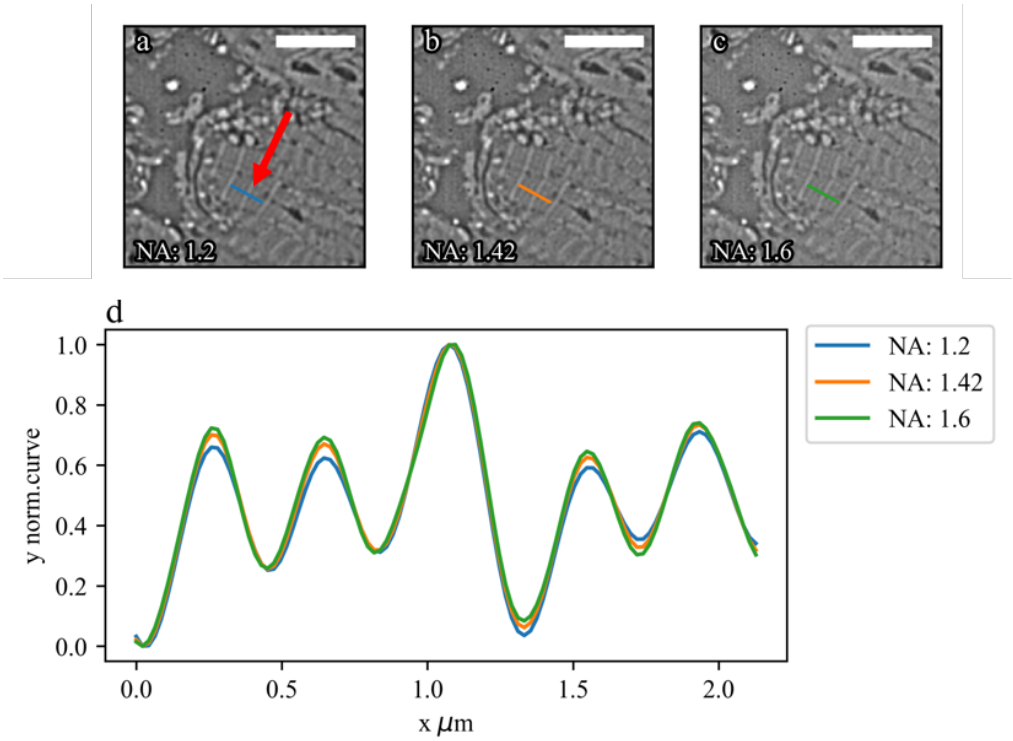

Fig. S4. Reconstructions using CE1s for heart tissue sample for different NA values that shows almost invariant results for incorrect value of NA. **a.** NA 1.2 (incorrect). **b.** NA 1.42 (correct). **c.** NA 1.6 (incorrect). **d.** Normalized profile for each case.

value. The reduced sensitivity to the incorrect NA in the indicator functions presented in this paper is attributed to the choice $b_i = 1$, which reduces the non-linearity of the indicator functions.

References

1. L. E. Villegas-Hernández, M. Nystad, F. Ströhl, P. Basnet, G. Acharya, and B. S. Ahluwalia, "Visualizing ultrastructural details of placental tissue with super-resolution structured illumination microscopy," Placenta **97**, 42–45 (2020).
2. J.-C. Tinguely, Ø. I. Helle, and B. S. Ahluwalia, "Silicon nitride waveguide platform for fluorescence microscopy of living cells," Opt. Express **25**, 27678–27690 (2017).
3. A. Mittal, A. K. Moorthy, and A. C. Bovik, "No-reference image quality assessment in the spatial domain," IEEE Transactions on Image Process. **21**, 4695–4708 (2012).
4. K. Agarwal and R. Macháň, "Multiple signal classification algorithm for super-resolution fluorescence microscopy," Nat. Commun. **7**, 13752 (2016).